

# Structure of the icosahedral Ti-Zr-Ni quasicrystal

R. G. Hennig\*

*Department of Physics, Ohio State University, Columbus, OH 43210, USA*

K. F. Kelton and A. E. Carlsson

*Department of Physics, Washington University, St. Louis, MO 63130, USA*

C. L. Henley

*Laboratory of Atomic and Solid State Physics, Cornell University, Ithaca, NY 14853, USA*

(Dated: July 28, 2021)

The atomic structure of the icosahedral Ti-Zr-Ni quasicrystal is determined by invoking similarities to periodic crystalline phases, diffraction data and the results from *ab initio* calculations. The structure is modeled by decorations of the canonical cell tiling geometry. The initial decoration model is based on the structure of the Frank-Kasper phase *W*-TiZrNi, the 1/1 approximant structure of the quasicrystal. The decoration model is optimized using a new method of structural analysis combining a least-squares refinement of diffraction data with results from *ab initio* calculations. The resulting structural model of icosahedral Ti-Zr-Ni is interpreted as a simple decoration rule and structural details are discussed.

## I. INTRODUCTION

Quasicrystals are solids that combine long-range translational order with rotational symmetries that forbid *periodic* translational symmetry. To understand the physical properties of quasicrystals, and in particular, the conditions under which nature prefers quasiperiodic to periodic order, it is necessary to determine their atomic structure. The aperiodic nature of quasicrystals requires new methods for structural analysis. In spite of significant progress in recent years, the complete atomic structure of quasicrystals still remains an unsettled question.<sup>1</sup>

The purpose of this paper is to determine the atomic structure of the thermodynamically stable icosahedral TiZrNi quasicrystal (*i*-TiZrNi). Although this material is the best-ordered among the known Ti-based quasicrystals, only polycrystalline samples with small grain sizes are available, which limits the information available from diffraction experiments. Therefore this paper develops a new method for structural analysis, based on the real-space structure description, whereby (several kinds of) tiles fill space and each kind of tile receives an identical “decoration” by atomic species, just as unit cells do in ordinary crystallography.

The known quasicrystal structures fall into two main types.<sup>2</sup> In a Frank-Kasper type structure, neighboring atoms always form tetrahedra, and the constituent species divide into “small” atoms (with icosahedral coordination) or “large” atoms (with coordination number up to 16). In an Al-transition metal (Al-TM) structure, the transition metals are commonly surrounded by an icosahedron of Al, and Al atoms often form octahedra. In either type, icosahedral quasicrystals (and closely similar crystalline phases called “approximants”) may be built from large ( $\sim 50$  atom) clusters with icosahedral symmetry: the “Bergman cluster”<sup>3</sup> in the Frank-Kasper case, or the “Mackay icosahedron”<sup>4</sup> in the Al-TM case. The Ti-based class of quasicrystals appears to fall on the border-

line between the two main types<sup>2</sup>; thus, though *i*-TiMn and *i*-TiCr fall in the Al-TM class, our subject *i*-TiZrNi is of the Frank-Kasper type. In developing its structural model, we will take advantage of structural relationships to both the *i*-AlMnSi and the Frank-Kasper quasicrystals.

## A. Methods of Structural Investigation

Many thermodynamically stable quasicrystals such as *i*-AlCuFe<sup>5</sup>, *i*-AlPdMn<sup>6</sup>, and *d*-AlNiCo<sup>7</sup> within the Al-TM metal class, *i*-AlCuLi and *i*-MgZnRE (RE=rare earth)<sup>8,9</sup> in the Frank-Kasper class, as well as the new binary quasicrystal *i*-CdYb<sup>10</sup>, can be grown as single grains up to several millimeter size, which allows the measurement of single crystal diffraction data. (Of those mentioned, all except *i*-AlCuLi also exhibit long-range order, i.e., instrumentally sharp Bragg peaks.) Using a variety of procedures<sup>1,11,12</sup>, atomic structures have been refined for many of these quasicrystals, such as *i*-AlCuLi<sup>13,14,15</sup>, *i*-AlCuFe<sup>16,17,18</sup> and *i*-AlPdMn<sup>19,20,21</sup>.

All these structures were parametrized as cuts by a three-dimensional hyperplane through a density in a six-dimensional hyperspace.<sup>22,23,24</sup> The difficulty with the six-dimensional approach is that only an average structure can be determined and disorder in the quasicrystal can not be treated appropriately. This, combined with experimental limitations such as truncation effects, usually produces a small number of spurious atoms with unphysical coordination numbers or small interatomic separations in structural models. A purely crystallographic approach alone might, therefore, not be able to fix all the positions and chemical identities of the atoms in quasicrystalline structures. It is furthermore infeasible for quasicrystalline alloys with small grain sizes for which only powder diffraction data are available.

Additional experimental and theoretical data, such as

structural information from related approximant phases and results from total energy calculations, can be helpful in the development of realistic structure models for quasicrystals. To incorporate this information a real space approach is desirable.<sup>25,26</sup> A common real space approach to the structure of quasicrystals is the tiling decoration. One splits the structural analysis into two parts: (1) the problem of the determination of the correct tiling geometry, and (2) the atomic decoration of the tiles. An advantage of the decoration viewpoint is different calculations (*ab initio* LDA, pair-potentials, diffraction simulation) may be performed using periodic tilings ("approximants") with larger or smaller unit cells, depending on the calculation's computational burden, and the results can be compared or combined in a systematic fashion.

The first tiling-decoration approaches were based on similarities to periodic crystalline structures.<sup>2,4</sup> In later work energetic considerations were taken into account. Examples of such investigations are the work by Krajčič and Hafner who investigated the structure of the *i*-AlMgZn quasicrystal using a decoration of the three-dimensional Penrose tiling and pair potentials based on the pseudopotential theory.<sup>27</sup> Windisch et al. studied the atomic and electronic structure and the lattice dynamics of *i*-AlCuLi using molecular dynamics simulations and density-functional calculations of decorated Penrose and canonical cell tilings.<sup>28,29</sup> The structure of the (metastable) *i*-AlMn quasicrystal has been studied by Mihalkovič et al. using canonical cell tiling decorations and pairpotentials.<sup>26,30</sup> Recently Mihalkovič et al. investigated the structure of decagonal AlCoNi using Monte-Carlo calculations with tile updates.<sup>31</sup>

All these investigations are based on the energetics of structural models and do not incorporate diffraction data into the modeling process. To derive a reliable structural model of a quasicrystal, a combination of the crystallographic approach based on diffraction data with information from total energy calculations and relaxation studies is highly desirable. In this paper we present the first study combining a least-squares refinement of X-ray and neutron diffraction data with structural information obtained from *ab initio* relaxations for approximant structures.

## B. The Ti-Zr-Ni quasicrystal

Few studies have been performed for quasicrystalline alloys with grain sizes so small that only powder diffraction data are available. Early work was devoted to the metastable system *i*-AlMnSi.<sup>32,33,34</sup> Another class of such quasicrystals are the Ti-based icosahedral alloys. As early as 1985, Zhang et al.<sup>35</sup> discovered a metastable icosahedral phase in Ti-Ni-V. In the following years, further icosahedral phases in Ti-based alloys containing other 3d transition metals such as V, Cr, Mn, Fe, Co and Ni were found.<sup>36,37,38,39,40,41,42</sup> However, no stable quasicrystalline phase of this class has been discovered yet.

Investigations of projection-based models of the structure of the Ti-Mn quasicrystal by Phillips et al. using tight-binding recursion and pair-potential based energy calculations<sup>43,44</sup> showed that the Mackay clusters form the backbone of the structure. Furthermore small additions of Si and O, which are crucial for the formation of the Ti-Cr and Ti-Mn quasicrystal<sup>40,45</sup>, were found to energetically stabilize the structure.<sup>46</sup>

In this work the experimentally well-studied icosahedral Ti-Zr-Ni quasicrystal is considered. As early as 1990, Molokanov and Chebotnikov<sup>47</sup> discovered a metastable icosahedral phase in Ti-Zr-Ni and in 1997 a thermodynamically stable icosahedral Ti-Zr-Ni phase was discovered by Kelton et al.<sup>48</sup> The *i*-TiZrNi quasicrystal is formed by either rapid quenching or solid state transformation at temperatures of 500°C to 600°C, generally leading to a fine microstructure of quasicrystal and crystal phases. The icosahedral phase is rather disordered with a coherence length of about 350 Å, resulting in a small number of measurable structure factors. Therefore, an atomic structure determination by diffraction experiments alone is impossible. Consequently little is known about the atomic structure of *i*-TiZrNi.

There is hope of obtaining information on the atomic arrangement in *i*-TiZrNi by studying the structure of related periodic "approximants", meaning crystal structures whose unit cells are fragments of some quasicrystal. There are several competing periodic phases known in the Ti-Zr-Ni phase diagram. Besides the binary phases  $\alpha$ -TiZr,  $\delta$ -Ti<sub>2</sub>Ni<sup>49</sup> and *l*-Zr<sub>2</sub>Ni<sup>50</sup>, there are two ternary phases; a cubic Frank-Kasper type structure (*W*-phase) and a hexagonal Laves type phase  $\lambda$ -TiZrNi.<sup>51</sup> The structures of the *W*-TiZrNi phase, which can be interpreted as a Fibonacci 1/1 approximant of *i*-TiZrNi, and of the  $\lambda$ -TiZrNi phases were determined by a Rietveld refinement using X-ray diffraction and neutron scattering data. Structural details were confirmed by *ab initio* calculations.<sup>52,53,54</sup> The *W*-TiZrNi phase is closely related to the quasicrystal phase.<sup>52,55</sup> They both form at similar compositions and temperature ranges and grow with a coherent crystallographic orientation. EXAFS studies indicate a similar local structure in both phases.<sup>56</sup> The presence of a reversible phase transformation between the icosahedral phase and the *W*-phase at about 600°C indicates that *i*-TiZrNi is a low-temperature phase, in contrast to most other quasicrystals.<sup>57</sup> This opens the exciting possibility that an (aperiodic) *i*-TiZrNi quasicrystal, or a very similar large-cell crystal, could be a ground state phase.

## C. Contents of this paper

The goal of our work is to model the ideal structure of the *i*-TiZrNi quasicrystal. The energetic stability and electronic structure of approximants to the *i*-TiZrNi quasicrystals, as well as the competing phases, are the topics of a subsequent paper. In this paper we present a structural analysis of *i*-TiZrNi based on a new method, com-

binning powder diffraction data and information from *ab initio* calculations in form of a constrained least-squares analysis. In Section II the initial decoration model is derived. We base our structure on the canonical cell tiling geometry, which is introduced in Section II B. As our starting point an initial atomic decoration of the canonical cells is determined from the atomic structure of the 1/1 approximant  $W$ -TiZrNi (Sec. II C). The following Section III on the optimization of the decoration model is the core of the paper. The constrained least-squares method of refinement is introduced. This approach incorporates structural information from *ab initio* relaxations as constraints into a least squares refinement of the diffraction data. The resulting structure can be understood as a simple decoration model. This and further details of the structural model, which are important for comparisons to experimental data such as EXAFS measurements, are discussed in Section IV.

## II. FIRST DECORATION MODEL

In this section we derive the initial decoration model. The underlying tiling geometry of our model is given by the canonical cell tilings. The canonical cell tilings provide a tiling model with a high packing fraction of icosahedral clusters. The location of the atomic sites decorating the canonical cells in our model are based on structural features of the  $W$ -phase.

### A. Structure of the $W$ -phase

The  $W$ -TiZrNi phase is a periodic crystalline phase closely related to the icosahedral quasicrystal. Its composition  $\text{Ti}_{50}\text{Zr}_{35}\text{Ni}_{15}$  is close to the composition of the quasicrystal  $\text{Ti}_{41.5}\text{Zr}_{41.5}\text{Ni}_{17}$  and it grows with a coherent crystallographic orientation with respect to the quasicrystalline phase. The structure of the  $W$ -phase was determined using X-ray diffraction and neutron scattering data and confirmed by *ab initio* calculations.<sup>52,53</sup>

It consists of a body centered cubic packing of icosahedral Bergman clusters connected by a few “glue” sites (see Table I). The Bergman cluster as shown in Figure 1 is composed of a central Ni atom surrounded by a small icosahedron of 12 Ti atoms. A second icosahedron is formed by placing 12 Ni atoms directly outside the vertices of the small icosahedron. Finally 20 Zr atoms are placed on the faces of the large icosahedron. The remaining 36 “glue” sites consist of 24 Ti atoms, forming a hexagon that separates the Bergman clusters along the threefold  $\langle 111 \rangle$  directions, and 12 Ti and Zr atoms, forming a rhombus that divides the Bergman clusters along the twofold  $\langle 100 \rangle$  directions. The structural analysis and *ab initio* calculations revealed that chemical disorder in the  $W$ -phase is abundant only between the chemically similar Ti and Zr atoms on the “glue” sites but no disorder is found on the cluster sites.<sup>52</sup>

TABLE I: Crystallographic description of the phase  $W$ -TiZrNi<sup>52</sup> showing the chemical occupation of the lattice sites. The positions of the sites are given in units of the lattice constant.

cI162		Space group Im $\bar{3}$			$a_o = 14.30 \text{ \AA}$
Site		$x$	$y$	$z$	Occupancy
1	$\alpha_1$	0	0	0	Ni(1.0)
2	$\beta_1$	0	0.103	0.165	Ti(1.0)
3	$\alpha_2$	0	0.193	0.310	Ni(1.0)
4	$\gamma_1$	0.186	0.186	0.186	Zr(1.0)
5	$\gamma_1$	0	0.307	0.114	Zr(1.0)
6	$\delta_1$	0.204	0	0.5	Zr(0.6), Ti(0.4)
7	$\delta_2$	0.145	0.187	0.401	Ti(1.0)
8	$\beta_2$	0.412	0	0.5	Zr(0.5), Ti(0.5)

The atomic structure of the  $W$ -phase is similar to the structure of the Frank-Kasper phases  $\text{Al}_{40}\text{Mg}_{40}\text{Zn}_{20}$ <sup>3</sup> and  $\text{Al}_{56}\text{Li}_{32}\text{Cu}_{12}$ <sup>58</sup>. The  $W$ -TiZrNi structure differs from these in (i) the occupation of the central site of the Bergman cluster, which is empty in the cases of Al-Mg-Zn and Al-Li-Cu, and (ii) the chemical disorder, which occurs between the smaller components Al and Zn or Cu in Al-Mg-Zn and Al-Li-Cu respectively and between the larger components Ti and Zr in the case of Ti-Zr-Ni. Furthermore, the analysis for  $i$ -TiZrNi showed chemical ordering on the sites of the Bergman cluster.

### B. Canonical cell tiling

In modeling the quasicrystal structure the canonical-cell tiling (CCT) model is used.<sup>59</sup> The packing rules permit periodic, random and in principle quasiperiodic tilings, although no rule for a quasiperiodic tiling has been found yet.<sup>26,59</sup> A large number of periodic approximants structures, ranging from a 1/1 up to a 31/24 approximant, are known for this tiling. In order to use the CCT’s for a structural description of quasicrystals and for a refinement of decoration models to experimental diffraction data, predictions for the structure factors of the icosahedral structure are needed (see App. A and B).

Canonical cell tilings consist of four kinds of disjoint cells denoted  $A$ ,  $B$ ,  $C$  and  $D$ . Their nodes are joined by two types of linkages,  $b$  and  $c$  bonds, which run in twofold and threefold symmetry directions respectively (see Fig. 2). There are three different kind of cell faces. The  $X$  face has the shape of an isosceles triangle formed by one  $b$  bond and two  $c$  bonds, the  $Y$  face with a shape of an equilateral triangle is formed by three  $c$  bonds and finally the rectangular  $Z$  face is formed by two  $b$  bonds and two  $c$  bonds.

The simplest quasiperiodic tiling with icosahedral symmetry is the Penrose tiling. Its tiles are the prolate rhombohedron ( $PR$ ) and oblate rhombohedron ( $OR$ ); their edges have the length  $a_q$  and run into fivefold symmetry directions. The CCT can uniquely be decomposed into  $PR$ ’s,  $OR$ ’s and rhombic dodecahedra consisting of

two  $PR$  and two  $OR$ .<sup>26,59</sup> A rhombic dodecahedron is assigned to each  $b$  bond and a  $PR$  to each  $c$  bond. They are called  $RD$  and  $PR_c$  respectively (see Fig. 3). They both connect nodes of the CCT.

Each triangular  $Y$  face is pierced by another kind of  $PR$ , which we will call  $PR_Y$ . It is useful to divide these  $PR_Y$  into two subclasses, called  $PR_Y(C)$  and  $PR_Y(D)$  according to whether it lies mostly in a  $C$  or  $D$  cell respectively. Each  $D$  cell contains three more  $PR$ 's, called  $PR_D$ . Finally, each  $Z$  face contains an  $OR$ . This decomposition of the CCT facilitates the description of the decoration model in the following section.

### C. Decoration description

We now derive the initial decoration sites for the canonical cell tiles from the structure of the  $W$ -phase. As our starting point we require that our decoration model reproduces the features of the  $W$ -TiZrNi structure wherever possible.

The structure of the  $W$ -phase corresponds to a Fibonacci 1/1 approximant. In the canonical cell tiling description the 1/1 approximant is given by an  $A_6$  tiling. The decoration of the  $A$ -cell is thus completely determined by the  $W$ -phase. The nodes of the  $A_6$  tiling correspond to the center of the Bergman cluster in the  $W$ -phase. Thus every node of the CCT will be occupied by a two-shell Bergman cluster and the atomic configuration surrounding the twofold ( $b$ ) and threefold ( $c$ ) linkages will be the same as in the  $W$ -phase. This already accounts for over 80% of the atoms in decoration of large tilings. We then extend our decoration model to the interior of the larger  $B$ ,  $C$  and  $D$  cells using the structure of  $W$ -TiZrNi as a guide.

We use the decomposition of the larger canonical cell tiles into prolate and oblate rhombohedron as well as the rhombic dodecahedron to describe their decoration. Since the  $A_6$  tiling can be decomposed into  $PR_c$ 's and  $RD$ 's, their atomic decoration is determined by the atomic structure of the 1/1 approximant (see Fig. 4). Simply to limit the number of free parameters, it is assumed that the decoration sites of the  $PR_Y(C)$ ,  $PR_Y(D)$  and  $PR_D$  are the same as for the  $PR_c$ . As for the  $OR$ , its face decoration is forced by the need to adjoin with the other tiles and it has no space for additional interior atoms (see Fig. 4). It is noted here that the site list is the same as for the Henley-Elser decoration of Al-Mg-Zn.<sup>2</sup>

After defining the general sites of the decoration model, the nomenclature for the different sites, necessary for a description of the chemical decoration, is introduced. From the  $W$ -phase we derived four general types of decoration sites for the Amman tiles. These are the vertices and the mid-edge sites of the Amman tiles, the two diagonal sites of the  $PR$ , and the sites inside of the  $RD$ . We denote these four kinds of sites by the letters  $\alpha$ ,  $\beta$ ,  $\gamma$  and  $\delta$  respectively (see Fig. 4). Any further differentiation of the sites is indicated by a subscript. The physical sig-

nificance is that identically labeled sites have the same coordinates and occupations in the decoration model.

The center and the second shell icosahedron of the Bergman cluster decorate vertices of the Amman tiles; these are denoted  $\alpha_1$  and  $\alpha_2$  respectively. The sites of the first shell of the Bergman cluster are equivalent to edge centers of the Amman tiles and are denoted by  $\beta_1$ . The  $PR_c$  has six mid-edge  $\beta_2$  sites on the plane bisecting its long axis. The two atomic sites on the long axis of the  $PR_c$  which, furthermore, also decorate the faces of the large icosahedron of the Bergman cluster, are denoted by  $\gamma_1$ . The same  $\gamma_1$  site also appears in the interior of the  $RD$ . There are four additional sites in the interior of the  $RD$  on the plane bisecting its long axis. These four sites form a rhombus. The sites on its short axis are denoted by  $\delta_1$  and the sites on its long axis by  $\delta_2$ . All of the decoration sites discussed up to now were directly derived from the structure of the  $W$ -phase.

For the  $B$ ,  $C$  and  $D$  cell we assume that the local structure is similar, with the decoration of the nodes and the  $b$  and  $c$  bonds the same as derived from the  $W$ -phase. There are additional sites which need to be specified for the  $B$ ,  $C$  and  $D$  cell. These are the sites connected to the  $PR_Y(C)$ , the  $PR_Y(D)$ , the  $PR_D$  and the  $OR$ . The acute vertex of the  $PR_Y$  closest to the  $Y$  face, the three mid-edges sites adjacent to this vertex and the adjacent site on the threefold axis are not already determined by adjacent tiles. These sites are called  $\alpha_3$ ,  $\beta_3$  and  $\gamma_2$  respectively (see Fig. 5(a)). For the  $PR_Y(D)$ , a number of sites inside the  $D$  cell must be specified. Starting from the acute vertex away from the  $Y$  face, the three mid-edge sites  $\beta_5$ , the three vertices  $\alpha_4$ , and the ring of six mid-edge sites  $\beta_6$  need to be specified. Furthermore, the site along the diagonal that is adjacent to the acute vertex that is away from the  $Y$  face is denoted by  $\gamma_3$  (see Fig. 5(c)). For the  $OR$ , the mid-edge sites are labeled  $\beta_4$  (see Fig. 5(d)). Along the diagonal of the  $PR_D$ , the site away from the node of the  $D$  cell is called  $\gamma_4$ . The six mid-edge sites on the plane bisecting the  $PR_D$  are denoted  $\beta_7$  (see Fig. 5(b)).

### III. STRUCTURAL REFINEMENT

In this section the decoration model for  $i$ -TiZrNi is optimized using a constrained least-squares analysis of diffraction data incorporating results from *ab initio* calculations. In this approach, the optimization of the structural model is split into two steps. In the first step, the chemical decoration of the atomic sites is refined by X-ray and neutron diffraction data while the site positions are kept fixed. The atomic positions are then optimized in a second step by *ab initio* relaxations of the resulting atomic decoration for periodic tilings. These relaxed atomic positions are then used as a constraint to the refinement of the diffraction data.

## A. Diffraction data

The sample preparation and the data acquisition was performed by E. H. Majzoub; details can be found in References [60,61]. The composition of the sample is  $(\text{Ti}_{41.5}\text{Zr}_{41.5}\text{Ni}_{17})_{98}\text{Pb}_2$ . The Pb was used, since it was assumed to accumulate in the grain boundaries due to its low solubility in the Ti-Zr-Ni phases. The regions to which the Pb segregates are liquid during the annealing, allowing for faster diffusion of the transition metals, thus enhancing the formation of larger quasicrystalline grains with longer coherence length. The samples were arc-melted from the pure materials under an argon atmosphere and then annealed at  $600^\circ\text{C}$  for 7 days under vacuum. The X-ray diffraction pattern was measured using  $\text{Cu-K}_\alpha$  radiation. Neutron powder diffraction data for the sample was obtained at the University of Missouri Research Reactor in collaboration with W. B. Yelon. The neutron wavelength was  $1.7675\text{\AA}$ .

The uncorrected structure factors were obtained from the powder diffraction data by performing a least-squares fit of the data to a Gaussian peak profile,

$$I(\theta) = I_b + I_0 \frac{1}{\sqrt{2\pi}\sigma} \exp\left(-\frac{(\theta - \theta_0)^2}{2\sigma^2}\right), \quad (1)$$

where the peak is centered at  $\theta_0$  and has a width of  $\sigma$ . The integrated intensity is given by  $I_0$ . Any peak broadening related to the diffractometer or the coherence length of the sample is absorbed in the width,  $\sigma$ , of the Gaussian peak profile. The data were fitted in a small interval of  $\Delta\theta \approx 1^\circ \dots 2^\circ$  around the center of each peak. The dependence of the results on the choice of the size of this interval was accounted for by the estimated errors, which reflect the range over which the fit parameters varied when the size of the interval over which the fit was performed was slightly changed. The background was fitted using a single parameter,  $I_b$ . Out of the 31 peaks for the neutron diffraction data, 24 peaks were indexed to the icosahedral phase and 7 were indexed to the  $\delta$ - $\text{Ti}_2\text{Ni}$  secondary phase. For the X-ray data, 18 structure factors were obtained. Three of the peaks belonged to the  $\delta$ - $\text{Ti}_2\text{Ni}$  secondary phase and 15 to the icosahedral quasicrystal.

Overall, the number of measured structure factors is rather small. Furthermore, since only powder diffraction data is available for the  $i$ -TiZrNi quasicrystal, a few of the measured structure factors were superpositions of crystallographically inequivalent reflections, further exacerbating a structural analysis. In the following two sections the initial decoration model for canonical cell tilings is refined to the measured structure factors constraining the atomic positions by *ab initio* relaxations.

## B. Calculating the structure factors

A least-squares analysis for the chemical decoration of the sites of the structure model to the X-ray

diffraction and neutron scattering data from icosahedral  $\text{Ti}_{41.5}\text{Zr}_{41.5}\text{Ni}_{17}$  was performed. As a good approximation of the quasiperiodic tiling, a cubic 8/5 CCT approximant with 576 nodes forming 1320  $A$ , 576  $BC$  and 136  $D$  cells containing 52392 atoms per unit cell and with a lattice constant of  $98\text{\AA}$  was used.<sup>62</sup> For the 8/5 approximant, the distribution of the complementary coordinates of the nodes has a small variance. It is thus reasonable to assume that this tiling is a good approximant to the hypothetical quasiperiodic canonical cell tiling. The decorations of the 8/5 canonical cell tiling were constructed using the *Canonical Cell Tiling Package* – “*There are the atoms*” by Mihalkovič.<sup>63</sup>

The icosahedral structure factor,  $F_{\text{ico}}(\mathbf{q})$ , is approximated by averaging over the amplitudes,  $F_{\text{app}}(\mathbf{q}_a)$ , of all the Bragg peaks in the approximant that map onto a single orbit of icosahedral peaks given by the wave vector,  $\mathbf{q}$ ,

$$F_{\text{ico}}(\mathbf{q}) = \frac{1}{M_{\text{ico}}(\mathbf{q})} \sum_a M_{\text{app}}(\mathbf{q}_a) F_{\text{app}}(\mathbf{q}_a). \quad (2)$$

Each corresponding orbit of reflections in the approximant is represented by a wave vector,  $\mathbf{q}_a$ , and has the multiplicity  $M_{\text{app}}$ .  $M_{\text{ico}}$  is the multiplicity of the icosahedral orbit. The average is taken over amplitudes instead of intensities requiring the correct choice of phases of the structure factors. It is therefore necessary to center the approximant structure in six dimensional space. Details of this and a discussion of the differences between averaging over amplitudes and intensities can be found in Appendices A and B.

The X-ray and neutron diffraction data were taken at room temperature. To account for thermal motion which decreases the structure factor,  $F_{\text{ico}}(\mathbf{q})$ , for large momentum,  $q$ , an isotropic Debye-Waller factor is used,

$$f_{\text{DW}}^s(q) = \exp\left(-\frac{B_{\text{iso}}^s}{8\pi^2} q^2\right). \quad (3)$$

Due to the small number of measured structure factors, only a single thermal parameter,  $B_{\text{iso}}^s$  with  $s \in \{\text{Ti}, \text{Zr}, \text{Ni}\}$ , for each atomic species was used. The X-ray form factors,  $f_s(q)$ , and the neutron scattering lengths,  $f_s$ , were taken from Reference [64].

Altogether the icosahedral structure factors,  $F_{\text{ico}}$ , needed for the refinement are given by

$$F_{\text{ico}}(\mathbf{q}) = \sum_{l,s} c_s(l) f_{\text{DW}}^s(q) f_s(q) \sum_a \frac{M_{\text{app}}(\mathbf{q}_a)}{M_{\text{ico}}(\mathbf{q})} \sum_{j \in \mathcal{L}_l} e^{i\mathbf{q}_a \cdot \mathbf{r}_j}. \quad (4)$$

The first sum is over all classes,  $l$ , of distinct sites of the decoration model. The second sum is over the three different atomic species,  $s \in \{\text{Ti}, \text{Zr}, \text{Ni}\}$ , decorating these classes of sites with concentrations,  $c_s(l)$ . The third summation is over the orbits of the approximant structure represented by the wave vector,  $\mathbf{q}_a$ , which correspond to the icosahedral wave vector,  $\mathbf{q}$ . Finally the last summation is taken over the individual atomic site,  $\mathbf{r}_j$ , belonging to the set of sites,  $\mathcal{L}_l$ , of the site class,  $l$ .

### C. Constrained least-squares refinement

Before we can compare the experimental peak intensities to the calculated structure factors, several correction factors have to be taken into account. For both, the X-ray and the neutron diffraction data, the intensities must be corrected by the Lorentz factor,  $\sec\theta \operatorname{cosec}^2\theta$ . Furthermore for the X-rays, the intensities are modified by the polarization,  $P$ , of the beam as described by the Thomson formula

$$\frac{1 + P \cos^2(2\theta)}{1 + P}. \quad (5)$$

Since the X-ray beam was unpolarized,  $P = 1$  is used. Overall the estimated intensity of a reflection is given by

$$I_{\text{ico}}(q) = \frac{1 + P \cos^2(2\theta)}{(1 + P)(\cos\theta \sin^2\theta)} |F_{\text{ico}}(q)|^2 \quad (6)$$

for X-ray diffraction and by

$$I_{\text{ico}}(q) = \sec\theta \operatorname{cosec}^2\theta |F_{\text{ico}}(q)|^2 \quad (7)$$

for neutron scattering.

Since the positions of the atoms are kept fixed in the refinement, the last two summations in Equation (4) over the atomic sites of each class with identical atomic decoration and over the orbits of wave vectors for the approximant are performed beforehand for all necessary values of  $\mathbf{q}_{\text{ico}}$ . The total structure factor for each  $\mathbf{q}$  was then obtained by summing over these partial structure factors multiplied by the average form factor or scattering length,  $f_s(q)$ , and the average Debye-Waller factor of the atoms decorating the site. The corrected intensity,  $I_{\text{ico}}$ , is then obtained from the calculated structure factor,  $F_{\text{ico}}$ , using Equations 6 or 7 respectively.

From the calculated intensities, the residuals  $R$  and  $R_w$  as well as the reduced  $\chi^2$  are obtained, providing a standard measure of how well the calculated data matches the observed one. The residuals are defined as

$$R = \frac{\sum_q \left| \sqrt{I_{\text{exp}}(q)} - \sqrt{I_{\text{ico}}(q)} \right|}{\sum_q \sqrt{I_{\text{exp}}(q)}} \quad (8)$$

and

$$R_w = \sqrt{\frac{\sum_q w(q) \left( \sqrt{I_{\text{exp}}(q)} - \sqrt{I_{\text{ico}}(q)} \right)^2}{\sum_q w(q) I_{\text{exp}}(q)}} \quad (9)$$

where the sums are over all observed and calculated intensities,  $I_{\text{exp}}$  and  $I_{\text{ico}}$  respectively. The weights  $w$  are given by the uncertainty of the measured intensities where  $w = 1/\sigma_I^2$ . The ‘‘goodness’’ of the fit is given by the reduced  $\chi^2$ ,

$$\chi^2 = \frac{\sum_q w(q) \left( \sqrt{I_{\text{exp}}(q)} - \sqrt{I_{\text{ico}}(q)} \right)^2}{N - N_p}, \quad (10)$$

where  $N$  is the total number of reflections and  $N_p$  is the number of estimated parameters.

Since the number of measured reflections is rather small, additional measured quantities such as the composition of the structure can be incorporated as constraints to the refinement and to limit the parameter space. The composition of the refined structure,  $c_i$ , was constrained by a penalty function,

$$\sum_{i \in \{\text{Ti, Zr, Ni}\}} (c_i - c_i^o)^2 / \sigma_c^2. \quad (11)$$

In order to ensure that the composition of the refined structure,  $c_i$ , does not deviate by more than a few percent from the nominal experimental value,  $c_i^o$ , a value of  $\sigma_c = 0.02$  was used. The  $\chi^2$  was then minimized by varying the chemical decoration of the sites using Powell’s conjugate direction method.<sup>65</sup>

The chemical decoration of the ideal atomic sites is refined with respect to the structure factors of 38 reflections for *i*-TiZrNi, 15 X-ray and 23 neutron diffraction structure factors. The maximum number of different sites of the decoration model is 18. The decoration of the sites in the *W*-phase structure was used for the initial configuration, i.e.  $\alpha$  sites were decorated with Ni,  $\beta$  sites with Ti and  $\gamma$  and  $\delta$  sites with Zr. The chemical decoration on each of these site classes was allowed to vary between two components, either Ti and Zr or Ti and Ni. About a dozen different starting configurations were used. The majority of the optimization runs resulted in the same final concentrations and gave the lowest observed  $\chi^2$ . However, as common in optimization problems, we cannot guarantee to have found the global minimum. During the refinement classes of sites which showed similar chemical occupancies were combined into a single class. The final number of independent classes of sites was six. This, and the three thermal parameters yield a total of nine estimated parameters.

The refinement using the initial decoration sites yielded for the residuals,  $R$ , of the structure factors 11.5% for X-ray, 6.1% for neutron and 6.9% combined. The weighted residuals,  $R_w$ , are 15.7% for X-ray, 4.6% for neutron and 5.7% combined. The reduced  $\chi^2$  is 1.8 indicating crystallographic significance for the fit. The thermal parameters for Ti and Zr,  $B_{\text{iso}}^{\text{Ti}} = 1.1\text{\AA}^2$  and  $B_{\text{iso}}^{\text{Zr}} = 1.2\text{\AA}^2$ , are comparable to values found in the  $\delta$ -(Ti,Zr)<sub>2</sub>Ni alloys.<sup>66</sup> The thermal parameter for Ni,  $B_{\text{iso}}^{\text{Ni}} = 2.3\text{\AA}^2$ , is about a factor two larger than the value found in  $\delta$ -(Ti,Zr)<sub>2</sub>Ni. This could reflect static disorder on some of the Ni sites.

### D. *Ab initio* relaxations

So far we have only refined the chemical decoration of the ideal sites of the canonical cell tiling. In the next step we perform *ab initio* relaxations for the resulting structure to investigate the site positions. The *ab initio*

calculations were performed with VASP<sup>67,68,69</sup>, which is a density functional code using a plane-wave basis and ultrasoft Vanderbilt-type pseudopotentials<sup>70,71</sup>. Atomic-level forces are calculated and relaxations with a conjugate gradient method are performed. *Ab initio* calculations are computationally very expensive. Thus, only calculations for small systems with up to a few hundred atoms are feasible on current computers. Therefore, *ab initio* relaxations only for the small periodic tilings of the canonical cells were performed. The tilings used were the  $A_6$ , the  $B_2C_2$  and the  $D_2$  tiling.<sup>59</sup>

As a starting configuration, the results from the analysis of the diffraction data were used. The chemical order was idealized by placing only the majority species on each site. The calculations were performed using the generalized gradient approximation by Perdew and Wang<sup>72</sup>, and a plane-wave kinetic-energy cutoff of  $E_{cut} = 302.0$  eV was chosen to ensure convergence. The pseudopotentials for Ti and Zr describe, besides the usual outer shell states, also the 3p and 4p states, respectively, as valence states. Due to the size of the quasicrystal-like tiling structures a check of the convergence with the number of k-points was not always possible due to computational limitation. Therefore the k-point mesh was chosen as large as possible, i.e.  $3 \times 3 \times 3$  for the  $A_6$  tiling,  $2 \times 2 \times 2$  for the  $B_2C_2$  tiling and  $1 \times 1 \times 1$  for the  $D_2$  tiling, corresponding to 4, 2 and 1 k-points in the irreducible part of the Brillouin zone respectively. The positions of the atoms, as well as the shape and volume of the unit cells, were relaxed until the total electronic energy change was smaller than 1 meV. This corresponds to atomic-level forces  $F_{max} \leq 0.02$  eV/Å.

TABLE II: Maximum and average displacements in [Å] of the atoms from their ideal positions for the different periodic canonical cell tilings after relaxation.

Tiling	Atoms	Displacement	
		average (rms)	max
$A_6$	81	0.10	0.19
$B_2C_2$	91	0.11	0.22
$D_2$	123	0.13	0.25

The atomic positions after the *ab initio* relaxation were remarkably close for all three tilings to the ideal atomic positions, such as the corners, mid-edges etc. of the decorated tiles, with average displacements smaller than 0.13 Å (see Table II).

The resulting atomic positions from the relaxation calculations were then symmetrized. This involves mapping the relaxed positions back onto their canonical orbit and calculating the average canonical coordinates of equivalent atoms.<sup>30,63</sup> The deviations of the relaxed atomic positions from their canonical coordinates are in general rather small with an average deviation of 0.07 Å. The largest deviation occurs for the  $\beta_4$  site, where the relaxed positions deviates by 0.19 Å in the  $D_2$  and by 0.05 Å in

TABLE III: Results of the refinement of the chemical decoration for the quasicrystal using the relaxed atomic positions.

Site	Description	Decoration	Class
$\alpha_1$ Cluster	Center	Ni (1.0)	1
$\beta_1$	Small icosahedron	Ti (1.0)	2
$\alpha_2$	Large icosahedron	Ni (1.0)	1
$\gamma_1$	Faces	Zr (1.0)	3
$\delta_1$ $b$ -bond	$RD$ Close pair	Zr (1.0)	3
$\delta_2$	$RD$ Distant pair	Zr (1.0)	3
$\beta_2$ $c$ -bond	$PR_c$ Mid edge	Ti (0.8) Zr (0.2)	4
$\alpha_3$ $Y$ -face	$PR_Y(C)$ Vertex	Ni (1.0)	1
$\beta_3$	$PR_Y(C)$ Mid-edge	Ti (1.0)	2
$\gamma_2$	$PR_Y(C)$ Upper diagonal	Ti (0.6) Zr (0.4)	5
$\beta_4$ $Z$ -face	$OR$ Mid-edges	Ni (0.7) Ti (0.3)	6
$\gamma_3$ $D$ -cell	$PR_Y(D)$ Lower diagonal	Zr (1.0)	3
$\alpha_4$	$PR_Y(D)$ Vertices	Ni (1.0)	1
$\beta_7$	$PR_Y(D)$ Mid-edges	Ti (1.0)	2
$\gamma_4$	$PR_D$ Diagonal	Ti (1.0)	2
$\beta_5$	$PR_D$ Mid-edges	Ti (1.0)	2
$\beta_6$	$PR_D$ Mid-edges	Ti (1.0)	2

the  $B_2C_2$  cell. In fact, the deviations in both cells have almost opposite directions.

The symmetrized positions are used as an input for fitting the site chemistry to the diffraction data. This process can, in principle, be repeated until convergence is achieved. In our case, since no significant changes in the decoration were observed, the optimization was already converged after the refinement of the relaxed atomic positions.

Using the relaxed positions, the residuals,  $R$ , of the structure factors decrease to 10.8% for X-ray, 5.1% for neutron and 5.9% combined. The weighted residuals,  $R_w$ , are 15.0% for X-ray, 4.0% for neutron and 5.1% combined. The reduced  $\chi^2$  is 1.4, indicating a good agreement between the calculated and measured structure factors (see Fig. 6). Overall, the relaxed positions lead to a better agreement with the diffraction data than the unrelaxed positions.

The resulting chemical decoration is given in Table III. The thermal parameter decreases for Ti to  $0.3\text{Å}^2$ , for Zr to  $1.0\text{Å}^2$  and it is unchanged for Ni. The chemical decorations on the sites change by less than 5%, with the exception of site  $\gamma_2$ , where the probability of finding Ti increases by 10%, and the site  $\alpha_4$ , that is now only occupied by Ni. The stoichiometry changes by less than 0.5%. The composition of the refined structure  $\text{Ti}_{41}\text{Zr}_{40}\text{Ni}_{19}$  agrees with the nominal composition  $\text{Ti}_{41.5}\text{Zr}_{41.5}\text{Ni}_{17}$  to within 2%.

This is the first refinement that systematically combines diffraction data and structural energies. Since the powder diffraction data for *i*-TiZrNi are not available for sufficiently high momentum  $q$  to usefully constrain the

coordinates the atomic positions were fixed to the results from *ab initio* relaxations. If better data were available for this quasicrystal, positional information would be available from the diffraction data as well. The relaxed atomic positions lead to an improved agreement between the calculated and measured structure factors. This illustrates that results from *ab initio* relaxations can successfully be incorporated as constraints into structural refinements.

#### IV. STRUCTURAL FEATURES OF THE QUASICRYSTAL

In this section we discuss some details of the resulting structural model for *i*-TiZrNi using the large 8/5 approximant and compare to the structure of the *W*-phase. Results for pair correlation functions, coordination numbers and local atomic environments, which are important for comparisons to experimental data such as EXAFS, are given in Tables IV and V as well as Figure 7.

TABLE IV: Number and average distance of nearest neighbors in parentheses in [Å] in the *W*-phase ( $a=14.3\text{\AA}$ ).

Center	Ti	Zr	Ni	Total
Ti	4.91 (2.90)	5.12 (3.07)	2.00 (2.66)	12.03 (2.93)
Zr	7.97 (3.07)	1.76 (3.12)	2.75 (3.19)	12.48 (3.10)
Ni	6.37 (2.66)	5.63 (3.19)	0.00 (-)	12.00 (2.91)

TABLE V: Number and average distance of nearest neighbors in parentheses in [Å] in the 8/5 approximant model ( $a=98.0\text{\AA}$ ).

Center	Ti	Zr	Ni	Total
Ti	3.95 (2.88)	5.85 (3.04)	2.34 (2.67)	12.14 (2.92)
Zr	5.91 (3.04)	3.30 (3.02)	2.91 (3.13)	12.12 (3.06)
Ni	4.93 (2.67)	6.05 (3.13)	0.83 (2.70)	11.81 (2.91)

Figure 7 shows the partial pair-distribution functions for the 1/1 approximant phase, *W*-TiZrNi, and the 8/5-approximant. Tables IV and V list the numbers and average distances of nearest neighbors in both structures. The pair-correlation functions for the *W*-phase and the quasicrystal resemble another, corresponding to the similar local atomic structures of both phases. While the *W*-phase has no Ni-Ni nearest neighbors at all, the number of Ni-Ni neighbor pairs in the quasicrystal is rather small. Chemical disorder was found only on a small number of sites, apparently localized to the glue region between the Bergman cluster, similar to the *W*-TiZrNi approximant (see Tab. I). Results of recent investigations of the local atomic structure of the *W*-phase and the quasicrystal by EXAFS measurements<sup>56</sup> are consistent with the pair-distribution functions of the structural model developed here.

The features of the decoration model of the quasicrystal can be understood by the energetics of the interactions between the constituents. Ti and Zr atoms are completely miscible and exhibit a zero heat of mixing. Ti and Ni as well as Zr and Ni, on the other hand, have a strongly negative heat of mixing, indicating strong attractive interactions between these pairs. Thus, it is energetically favorable for all the Ni atoms to be surrounded by Ti or Zr. This explains why, in the structure of the 1/1 approximant and the quasicrystal, hardly any Ni-Ni bonds occur. Since Zr is slightly larger than Ti it is no surprise that Zr occupies the more open sites of the structure given by the interior of the *PR* and *RD*.

The refined structure of the quasicrystal is very similar to the structure of the 1/1 approximant phase, *W*-TiZrNi. The atomic sites for the structure model of the quasicrystal are based on the *W*-phase structure. The refined decoration of these sites is the same in most cases. However, the  $\delta_1$  and  $\delta_2$  sites along the *b* bond are occupied by Zr only in the quasicrystal, while in the *W*-phase chemical disorder occurs between Ti and Zr. Overall, the amount of chemical disorder in the quasicrystal appears to be of the same order or even slightly less than in the *W*-phase. Considering the apparent disorder in the powder diffraction patterns, the lack of chemical disorder on most sites of the structural model of the quasicrystal seems surprising at first and might be fortuitous. However, it is noted, that the quasicrystal forms at low temperatures, possibly reducing the amount of entropic disorder. We speculate, that an (aperiodic) *i*-TiZrNi quasicrystal, or a very similar large-cell crystal, could be a ground state phase. This idea is investigated in a subsequent paper.

#### V. CONCLUSION

We have developed the first realistic structural model for the icosahedral Ti-Zr-Ni quasicrystal. Our model is based on atomic decorations of the canonical cell tilings. For the structural refinement a new method of constrained least squares analysis is used, combining X-ray and neutron diffraction data with results from *ab initio* relaxations. The refined structural model exhibits only small amounts of chemical disorder between Ti and Zr.

This structural model should be helpful for a better understanding and interpretation of experimental data such as, for example, EXAFS data, pcT-isotherms, relations to crystalline phases and the ternary phase diagram. Furthermore this model will enable us to investigate the possibility of *i*-TiZrNi as a ground state quasicrystal.

#### Acknowledgments

The work at Washington University was supported by the National Science Foundation (NSF) under grants DMR 97-05202 and DMR 00-72787. Work at Cornell



made use of the Cornell Center for Materials Research Computing Facilities, supported through the National Science Foundation MRSEC program (DMR-0079992). C.L.H. was supported by the Department of Energy (DOE) grant DE-FG02-89ER-45405. R.G.H. was partially supported by NSF grant DMR-0080766 and by DOE grant DE-FG02-99ER45795. We thank Alex Quandt and Jeff Neaton for discussions about the VASP code, Marek Mihalkovič for the code to decorate canonical cell tilings and E. H. Majzoub for providing us with the X-ray and neutron diffraction data.

## APPENDIX A: DIFFRACTION FROM APPROXIMANTS

In this Appendix a method is presented for the calculation of the structure factors of the icosahedral quasicrystal from large cubic approximants.

Assuming that the local structure of the approximant closely resembles the structure of the quasicrystals, the quasicrystal structure factors can be approximated by the structure factors of a large periodic approximant. However, a direct comparison of the structure factors of the approximant to measured structure factors of the icosahedral phase is not possible due to the different symmetries of the structures. This leads to different multiplicities of corresponding reflections for both structures and a splitting of orbits of icosahedral reflections in the case of the approximant. The problem is further complicated by the fact that the Bragg reflections of the quasicrystal form a dense set, which is not the case for the periodic approximants. Inequivalent low intensity reflections, therefore, can become degenerate in the approximant. The problem of degenerate reflections in the approximant becomes increasingly important in smaller approximants. Since, for structural investigations only Bragg reflections with intensities above a threshold are used, the degeneracy problem can be avoided by using a large enough approximant.

The six dimensional representation of icosahedral quasicrystals enables one to relate their diffraction patterns to the diffraction patterns of their related crystalline approximants. The reciprocal lattice (RL) of the approximant is obtained when the golden mean,  $\tau$ , which appears in the icosahedral basis of the physical space, is replaced by the rational number  $\tau_n = f_{n+1}/f_n$ . The mapping of the icosahedral RL to the cubic RL is induced by keeping the same six indices but using the rationally related basis vectors. Every icosahedral reciprocal lattice vector (RLV) maps to a unique cubic RLV. The maximum cubic subgroup of the icosahedral symmetry group,  $m\bar{3}5$ , is given by  $m3$ . While the order of the icosahedral group is 120, the order of the cubic subgroup is only 24. Thus, the image of one orbit of equivalent icosahedral reflections is the union of up to five cubic orbits. Although an icosahedral RLV vector does not map to a cubic RLV in the same direction, any icosahedral RLV in a given

fundamental domain of the cubic group maps to a cubic RLV in the same fundamental domain. Thus, to get the standard representative cubic RLV's corresponding to one icosahedral RLV orbit, we only need to check the images of all icosahedral RLV's in that orbit whose orientations fall in the standard principal triangle of the cubic group.

The calculation of the structure factors for the icosahedral phase from the cubic approximant proceeds in two steps. First, for every orbit of icosahedral reflections with complementary components smaller than some cutoff,  $Q_{\max}^{\perp}$ , the multiplicity,  $M_{\text{ico}}$ , is determined by analyzing if the representing RLV points into any high-symmetry direction of the icosahedral point group. The icosahedral RLV's of the orbit which fall into the fundamental domain of the cubic point group are determined. Depending on the multiplicity of the icosahedral orbit this results in a set of up to five RLV's. For each of these icosahedral RLV, the corresponding cubic RLV in the approximant is determined by the projection method, where the golden mean,  $\tau$ , in the basis vectors of the physical space is replaced by the rational approximant,  $\tau_n$ . The multiplicity,  $M_a$ , of the orbit represented by each of the cubic RLV's is calculated by analyzing if the cubic RLV points into any high-symmetry direction of the cubic point group.

In the second step, to approximate the structure factor of the icosahedral RLV, the structure factors of the corresponding cubic RLV's of the periodic approximant are calculated and averaged. This average could be taken over either the amplitudes or the intensities of the structure factors. While for reflections with a high intensity, both methods of averaging result in nearly the same values, for low intensity reflections the right choice of averaging is more important. Since all the cubic approximants are centrosymmetric, the structures can be centered such that the phases of the structure factors are either 0 or  $\pi$ , resulting in a plus or minus sign for the structure factors. The correct centering of the approximant structures involves a shift in the six-dimensional space. The 1/1 approximant structure requires no shift. For the cubic 2/1, 3/2, 8/5 and 13/8 approximants of the canonical cell tiling, the six-dimensional centering vector is given by  $\frac{1}{2}(1, 0, 1, 1, 0, 0)$ . These approximants have the symmetry group  $Pa\bar{3}$ . That means that there is one 3-fold axis which passes through the node at the origin in real space. That 3-fold axis is chosen to be in the cubic (111) direction which corresponds to the six-dimensional vector  $(1, 0, 1, 1, 0, 0)$ .

For reflections with nearly vanishing intensity, the splitting of the reflection in the approximant leads to a distribution of structure factors around zero. An averaging over intensities would lead to a positive value, while for averaging over amplitudes the resulting value is closer to zero and provides a better approximation. In this work, the icosahedral structure factor is estimated by averaging over the amplitudes of the corresponding structure factors of a large cubic approximant (see Eqs. (2) and (4)). In order for the approximated structure factors

to closely resemble the icosahedral structure factors, the atomic structure of the approximant has to resemble the structure of the icosahedral phase closely, which is more likely the case for larger approximants.

## APPENDIX B: AVERAGING OVER AMPLITUDES OR INTENSITIES

To compare the accuracy of the prediction of the structure factors from averaging over amplitudes and over intensities the method is applied to the Penrose tiling, since for the ideal quasiperiodic Penrose tiling, the structure factors can be easily calculated by Fourier transformation of the acceptance domain. If the vertices of the Penrose tiling are identical scatterers, the structure factors of the ideal quasiperiodic Penrose tiling are determined by the

Fourier transformation of the triacontahedral acceptance domain.<sup>73</sup>

In Figure 8 the structure factors for the ideal quasiperiodic Penrose tiling are compared to the estimated values from the cubic Penrose 1/1 and 3/2 approximant structures. While for the 1/1 approximant the structure factors deviate strongly at lower intensities, already for the 3/2 approximants the estimated structure factors closely resemble the icosahedral structure factors over about three orders of magnitude. Averaging over amplitudes instead of intensities leads to significant improvements in the case of the 1/1 approximant, but only minor changes for the 3/2 approximant. It is noted here, that the Penrose tiling decorated with unit scatterers on the vertices is likely to oversimplify the problem and that in more realistically decorated structures, larger deviations could occur.

- 
- \* rhennig@mps.ohio-state.edu; URL: <http://www.physics.ohio-state.edu/~rhennig>
- <sup>1</sup> M. Boudard and M. de Boissieu, in *Physical Properties of Quasicrystals*, edited by Z. M. Stadnik (Springer: Berlin, Heidelberg, New York, 1999), vol. 126 of *Solid State Sciences*, pp. 91–126.
  - <sup>2</sup> C. L. Henley and V. Elser, *Philosophical Magazine B* **53**, L59 (1986).
  - <sup>3</sup> G. Bergman, J. L. T. Waugh, and L. Pauling, *Acta Crystallographica* **10**, 254 (1957).
  - <sup>4</sup> V. Elser and C. L. Henley, *Physical Review Letters* **55**, 2883 (1985).
  - <sup>5</sup> A. P. Tsai, A. Inoue, and T. Masumoto, *Japanese Journal of Applied Physics* **26**, L1505 (1987).
  - <sup>6</sup> A. P. Tsai, A. Inoue, Y. Yokoyama, and T. Masumoto, *Materials Transactions, JIM* **31**, 98 (1990).
  - <sup>7</sup> S. Ritsch, C. Beeli, H.-U. Nissen, T. Gödecke, M. Scheffer, and R. Lück, *Phil. Mag. Lett.* **74**, 99 (1996).
  - <sup>8</sup> A. Niikura, A. P. Tsai, A. Inoue, and T. Masumoto, *Philosophical Magazine Letters* **69**, 351 (1994).
  - <sup>9</sup> A. P. Tsai, A. Niikura, A. Inoue, T. Masumoto, Y. Nishida, K. Tsuda, and M. Tanaka, *Philosophical Magazine Letters* **70**, 169 (1994).
  - <sup>10</sup> A. P. Tsai, J. Q. Guo, E. Abe, H. Takakura, and T. J. Sato, *Nature* **408**, 537 (2000).
  - <sup>11</sup> W. Steurer and T. Haibach, in *Physical Properties of Quasicrystals*, edited by Z. M. Stadnik (Springer: Berlin, Heidelberg, New York, 1999), vol. 126 of *Solid State Sciences*, pp. 51–89.
  - <sup>12</sup> V. Elser, *Acta Crystallographica A* **55**, 489 (1999).
  - <sup>13</sup> A. Yamamoto, *Physical Review B* **45**, 5217 (1992).
  - <sup>14</sup> M. de Boissieu, C. Janot, J. M. Dubois, M. Audier, and B. Dubost, *Journal of Physics: Condensed Matter* **3**, 1 (1991).
  - <sup>15</sup> S.-Y. Qiu and M. V. Jaric, *Physical Review B* **52**, 894 (1995).
  - <sup>16</sup> M. Cornier-Quiquandon, A. Quivy, S. Lefebvre, E. Elkaim, G. Heger, A. Katz, and D. Gratias, *Physical Review B* **44**, 2071 (1991).
  - <sup>17</sup> A. Katz and D. Gratias, *Journal of Non-Crystalline Solids* **153-154**, 187 (1993).
  - <sup>18</sup> E. Cockayne, R. Phillips, X. B. Kan, S. C. Moss, J. L. Robertson, T. Ishimasa, and M. Mori, *Journal of Non-Crystalline Solids* **153&154**, 140 (1993).
  - <sup>19</sup> M. de Boissieu, P. Stephens, M. Boudard, C. Janot, D. L. Chapman, and M. Audier, *Journal of Physics: Condensed Matter* **6**, 10725 (1994).
  - <sup>20</sup> M. Boudard, M. de Boissieu, C. Janot, J. M. Dubois, and C. Dong, *Philosophical Magazine Letters* **64**, 197 (1991).
  - <sup>21</sup> C. Janot, M. de Boissieu, M. Boudard, H. Vincent, M. Durand, and J. M. Dubois, *Journal of Non-Crystalline Solids* **150**, 322 (1992).
  - <sup>22</sup> C. Janot, M. de Boissieu, J. M. Dubois, and J. Pannetier, *Journal of Physics: Condensed Matter* **1**, 1029 (1989).
  - <sup>23</sup> P. Bak, *Physical Review Letters* **56**, 861 (1986).
  - <sup>24</sup> D. Gratias, J. W. Cahn, and B. Mozer, *Physical Review B* **38**, 1643 (1988).
  - <sup>25</sup> C. L. Henley, V. Elser, and M. M. c, *Zeitschrift für Kristallographie* **215**, 553 (2000).
  - <sup>26</sup> M. Mihalkovič, W.-J. Zhu, C. L. Henley, and M. Oxborrow, *Physical Review B* **53**, 9002 (1996).
  - <sup>27</sup> M. Krajčič and J. Hafner, *Physical Review B* **46**, 10669 (1992).
  - <sup>28</sup> M. Windisch, J. Hafner, M. Krajčič, and M. Mihalkovič, *Physical Review B* **49**, 8701 (1994).
  - <sup>29</sup> M. Windisch, M. Krajčič, and J. Hafner, *Journal of Physics: Condensed Matter* **6**, 6977 (1994).
  - <sup>30</sup> M. Mihalkovic, W. J. Zhu, C. L. Henley, and R. Phillips, *Physical Review B* **53**, 9021 (1996).
  - <sup>31</sup> M. Mihalkovič, I. Al-Lehyani, E. Cockayne, C. L. Henley, N. Moghadam, J. A. Moriarty, Y. Wang, and M. Widom (2001), unpublished.
  - <sup>32</sup> M. Duneau and C. Oguey, *Journal de Physique France* **50**, 135 (1989).
  - <sup>33</sup> J. W. Cahn, D. Gratias, and B. Mozer, *Journal de Physique France* **49**, 1225 (1988).
  - <sup>34</sup> C. Janot, J. M. Dubois, M. de Boissieu, and J. Pannetier, *Physica B* **156 & 157**, 25 (1989).
  - <sup>35</sup> Z. Zhang, H. Q. Ye, and K. H. Kuo, *Philosophical Magazine A* **52**, L49 (1985).
  - <sup>36</sup> C. Dong, Z. K. Hei, L. B. Wang, Q. H. Song, Y. K. Wu, and K. H. Kuo, *Scripta Metallurgica* **20**, 1155 (1986).

- <sup>37</sup> K. F. Kelton, P. C. Gibbons, and P. N. Sabes, *Physical Review B* **38**, 7810 (1988).
- <sup>38</sup> R. A. Dunlap, R. C. O'Handley, M. E. McHenry, and R. Chatterjee, *Physical Review B* **37**, 8484 (1988).
- <sup>39</sup> J. C. Holzer, K. F. Kelton, and P. C. Gibbons, *Scripta Metallurgica* **23**, 691 (1989).
- <sup>40</sup> J. L. Libbert and K. F. Kelton, *Philosophical Magazine Letters* **71**, 153 (1995).
- <sup>41</sup> K. F. Kelton and X. Zhang, *Bulletin of the American Physical Society* **35**, 523 (1990).
- <sup>42</sup> X. Zhang and K. F. Kelton, *Philosophical Magazine Letters* **63**, 39 (1991).
- <sup>43</sup> R. Phillips, H. Deng, A. E. Carlsson, and M. S. Daw, *Physical Review Letters* **67**, 3128 (1991).
- <sup>44</sup> R. Phillips, H. Deng, A. E. Carlsson, and M. S. Daw, *Physical Review B* **45**, 7463 (1992).
- <sup>45</sup> X. Zhang and K. F. Kelton, *Philosophical Magazine Letters* **62**, 265 (1990).
- <sup>46</sup> R. G. Hennig and H. Teichler, *Philosophical Magazine A* **76**, 1053 (1997).
- <sup>47</sup> V. V. Molokanov and V. N. Chebotnikov, *Journal of Non-Crystalline Solids* **117-118**, 789 (1990).
- <sup>48</sup> K. F. Kelton, W. J. Kim, and R. M. Stroud, *Applied Physics Letters* **70**, 3230 (1997).
- <sup>49</sup> G. A. Yurko, J. W. Barton, and F. G. Parr, *Acta Crystallographica* **12**, 909 (1959).
- <sup>50</sup> M. E. Kirkpatrick, D. M. Bailey, and J. F. Smith, *Acta Crystallographica* **15**, 252 (1962).
- <sup>51</sup> V. V. Molokanov, V. N. Chebotnikov, and Y. K. Kovneristy, *Inorganic Materials*, translated from *Izvestiya Akademii Nauk SSSR, Neorganicheskie Materialy* **25**, 46 (1989).
- <sup>52</sup> R. G. Hennig, E. H. Majzoub, A. E. Carlsson, K. F. Kelton, C. L. Henley, W. B. Yelon, and S. Mixture, *Materials Science and Engineering A* **294-296**, 361 (2000).
- <sup>53</sup> W. J. Kim, P. C. Gibbons, K. F. Kelton, and W. B. Yelon, *Physical Review B* **58**, 2578 (1998).
- <sup>54</sup> E. H. Majzoub, R. G. Hennig, and K. F. Kelton, submitted to *Philosophical Magazine A* (2001).
- <sup>55</sup> W. J. Kim, P. C. Gibbons, and K. F. Kelton, *Philosophical Magazine Letters* **76**, 199 (1997).
- <sup>56</sup> A. Sadoc, J. Y. Kim, and K. F. Kelton, submitted to *Philosophical Magazine B* (2000).
- <sup>57</sup> J. P. Davis, E. H. Majzoub, J. M. Simmons, and K. F. Kelton, *Materials Science and Engineering A* **294-296**, 104 (2000).
- <sup>58</sup> M. Audier, J. Pannetier, M. Leblanc, C. Janot, J.-M. Lang, and B. Dubost, *Physica B* **153**, 136 (1988).
- <sup>59</sup> C. L. Henley, *Physical Review B* **43**, 993 (1991).
- <sup>60</sup> E. H. Majzoub, Ph.D. thesis, Washington University in St. Louis (2000).
- <sup>61</sup> E. H. Majzoub, J. Y. Kim, R. G. Hennig, K. F. Kelton, P. C. Gibbons, and W. B. Yelon, *Materials Science and Engineering A* **294-296**, 108 (2000).
- <sup>62</sup> M. Mihalkovič and P. Mrafko, *Europhysics Letters* **21**, 463 (1993).
- <sup>63</sup> M. Mihalkovič (2000), unpublished.
- <sup>64</sup> *International tables for crystallography* (Kluwer Academic, 1992), chap. 6.1.
- <sup>65</sup> W. H. Press, S. A. Teukolsky, W. T. Vetterling, and B. P. Flannery, *Numerical Recipes in C* (Cambridge University Press, 1993), Second ed.
- <sup>66</sup> R. Mackay, G. J. Miller, and H. F. Franzen, *Journal of Alloys and Compounds* **204**, 109 (1994).
- <sup>67</sup> G. Kresse and J. Hafner, *Physical Review B* **47**, 558 (1993).
- <sup>68</sup> G. Kresse and J. Furthmüller, *Computational Materials Science* **6**, 15 (1996).
- <sup>69</sup> G. Kresse and J. Furthmüller, *Physical Review B* **54**, 11169 (1996).
- <sup>70</sup> D. Vanderbilt, *Physical Review B* **41**, 7892 (1990).
- <sup>71</sup> G. Kresse and J. Hafner, *Journal of Physics: Condensed Matter* **6**, 8245 (1994).
- <sup>72</sup> J. P. Perdew and Y. Wang, *Physical Review B* **45**, 13244 (1992).
- <sup>73</sup> V. Elser, *Acta Crystallographica A* **42**, 36 (1986).

FIG. 1: Structure of the Bergman cluster consisting of a central Ni atom (left), a small icosahedron of Ti atoms (center) and a large icosahedron of Ni atoms with Zr atoms on the face centers (right).

FIG. 2: The four canonical cells. The b-bonds and c-bonds are represented by the double and single lines respectively. The face names are also indicated.

FIG. 3: Decomposition of the canonical cells tiling into prolate and oblate rhombohedra as well as the rhombic dodecahedron.

FIG. 4: Decoration of (a) the rhombic dodecahedron, (b) the prolate rhombohedron and (c) the oblate rhombohedron. The right-hand pictures show the same decorations with interiors visible.

FIG. 5: Decoration of (a) the  $PR_Y(C)$ , (b) the  $PR_D$ , (c) the  $PR_Y(D)$  and (c) the  $OR$ .

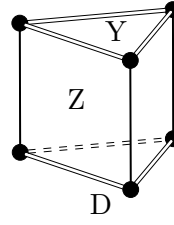
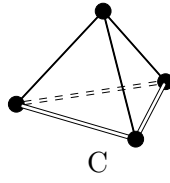
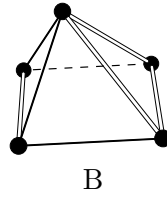
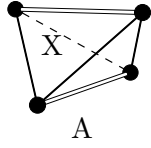
FIG. 6: Comparison of the experimental X-ray diffraction and neutron scattering data to the simulated diffraction of the icosahedral structure.

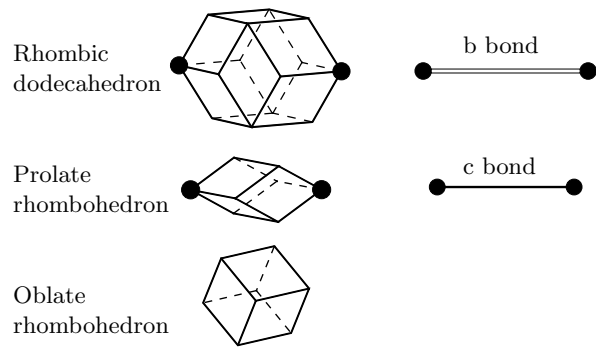
FIG. 7: Partial pair distribution functions of the  $W$ -phase (top) and the  $8/5$ -approximant model (bottom).

FIG. 8: Comparison of the structure factors of the icosahedral Penrose tiling to the estimated values from the periodic  $1/1$  and  $3/2$  approximants. The results from averaging over intensities is show in the top panels and for averaging over amplitudes in the bottom panels.

This figure "Figure1.png" is available in "png" format from:

<http://arxiv.org/ps/cond-mat/0202517v1>





This figure "Figure4.png" is available in "png" format from:

<http://arxiv.org/ps/cond-mat/0202517v1>



This figure "Figure5.png" is available in "png" format from:

<http://arxiv.org/ps/cond-mat/0202517v1>

